

Thermal Aspects for Composite Structures - From Manufacturing to In-Service Predictions[☆]

T. Sproewitz^a, Chr. Huehne^b, E. Kappel^b

^a*DLR, Institute of Space Systems, Robert-Hooke-Str. 7, 28359 Bremen, Germany*

^b*DLR, Institute of Composite Structures and Adaptive Systems, Lilienthalplatz 7, 38108 Braunschweig, Germany*

Abstract

Manufacturing of composite structures with a high degree of dimensional accuracy remains a challenge in modern fabrication. Residual stresses in fibre reinforced laminates which develop during the autoclav processing lead to a variety of process induced deformations. Dimensional changes such as spring-in of angled structures and warpage of flat sections are characteristic for composite manufacturing. This paper presents an engineering approach for a thermo-elastic simulation of the spring-in effect on large airframe structures based on the FE method performed at the DLR Institute of Composite Structures and Adaptive Systems. Due to the use of Ni36 as tooling material it was possible to blank out the influence of varying CTE between tool and part which are responsible for warpage. Investigations on small manufactured L-profiles with a flangelength of 50 mm deliver the necessary simulation parameters for the constitutive model of the relevant airframe structure. For estimating the influence of different autoclav processes on the amount of spring-in, investigations with different temperature profiles were conducted and will be presented.

Keywords: Composites, CTE, spring-in, thermo-elastic, aircraft structures

Nomenclature

$\Delta\theta$	spring-in angle [Deg]
θ	reference-angle [Deg]
θ'	actual-angle [Deg]
R	reference-radius [mm]
R'	actual-radius [mm]
t	reference-thickness [mm]
t'	actual-thickness [mm]
α_r	radial CTE [$\frac{1}{K}$]
α_t	tangential CTE [$\frac{1}{K}$]
ϕ_r	rad. chemical shrinkage [%]
ϕ_t	tang. chemical shrinkage [%]
$\Delta\theta_{th}$	thermal fraction angle [Deg]
$\Delta\theta_{ch}$	chemical fraction angle [Deg]
$\Delta\theta_{glob}$	global spring-in angle [Deg]
$\Delta\theta_{loc}$	local spring-in angle [Deg]
\tilde{T}	reference-temperature [K]
T	actual-temperature [K]
$T_{process}$	process-temperature [K]
p	pressure [MPa]
\tilde{p}	reference-pressure [MPa]
$p_{process}$	process-pressure [MPa]

ΔV_{chem}	chem. volume shrinkage [%]
$\alpha_{m_{chem}}$	chem. matrix shrinkage [$\frac{1}{K}$]
$\alpha_{m_{equ}}$	equivalent matrix shrinkage [$\frac{1}{K}$]
$\alpha_{m_{therm}}$	thermal matrix shrinkage [$\frac{1}{K}$]

1. Introduction

Because of their superior mechanical properties and high stiffness to weight ratio, fiber reinforced composites are increasingly used for primary aircraft structures. The manufacturing process of composite parts often leads to internal stresses which cause shape deformations of the part after demoulding. Taking into consideration manufacturing rates of more than 30 aircraft per month economic processes with a high degree of dimensional part accuracy are mandatory. Poor dimensional control leads to increasing assembly efforts and hence increasing costs. The production of highly integral structures may on the one hand reduce assembly costs but may on the other hand require sophisticated manufacturing processes. The ability to control dimensional accuracy demands further investigations concerning analysis methods and strategies. The prediction of material characteristics and thus the simulation of process induced deformations depends on a variety of parameters. Curing simulation requires consideration of transient temperature fields taking into account internal heat generation from chemical reactions of the matrix material. Thus it is the basis for the determination of the degree of cure and hence the chemical shrinkage. Optimization of process cycle (temperature levels, heating and

[☆]This document is a collaborative effort.

Email addresses: tom.sproewitz@dlr.de (T. Sproewitz), christian.huehne@dlr.de (Chr. Huehne), erik.kappel@dlr.de (E. Kappel)

URL: <http://www.dlr.de/irs> (T. Sproewitz), <http://www.dlr.de/fa> (Chr. Huehne), <http://www.dlr.de/fa> (E. Kappel)

cooling rates) can affect residual stresses. Thereby it has an influence on in-service predictions. Accurate simulation techniques, with regard to mentioned parameters, are mandatory for reliable manufacturing processes and hence the reduction of validation and testing efforts. Process Parameters influence the transformation from liquid to solid state of the matrix material significantly. Therefore scientists combined curing, thermal and residual stress analysis. Svanberg and Holmberg [1] developed a visco elastic material model taking into account relaxation of the matrix in rubbery state and established a link to the thermal analysis. Zhu and Geubelle [2] pursued a similar approach.

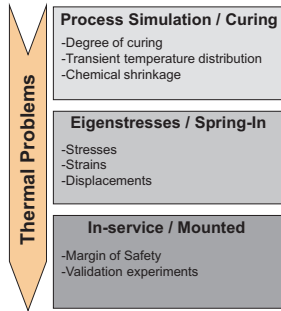


Figure 1: Thermal issues in manufacturing

Chemical shrinkage in direct relation to the degree of cure set up a link to residual stresses. Flores [3] compared several models for this relations and evaluated their applicability.

Darrow [4] and Sweeting [5] used linear static FE-analysis for the simulation of spring-in effects. Darrow combined thermal and chemical shrinkage properties to implement an equivalent CTE. Sweeting used the original CTE to model thermal expansion and prescribed strains to account for chemical shrinkage.

Fernlund et al. [6] investigated effects of design and process parameters on the two main kinds of deformation spring-in and warpage of angled thermoset laminates. He named four parameters to which he assigned high potential to affect the magnitude of shape deformations - tool surface, part length, part thickness and cure cycle. Svanberg [7] pursued an engineering approach using the FE-Code ABAQUS to predict shape distortions for a curved composite C-Spar. It shows good accuracy of cure induced shape deformations with regard to his assumptions and simplifications. However, it has already been shown, that a fast engineerlike spring-in estimation based on linear-static analysis with consideration of chemical shrinkage is a reasonable approach. Drawbacks of this combined analysis technique are:

- a sample test program for each material and process,
- the structure needs to be manufactured with the same process as the sample test program,
- assumption that the whole structure is homogeneously cured.

In the current study the determination of the magnitude of matrix shrinkage was conducted based on carbon fibre reinforced plastic L-profiles as shown in Figure 2. This kind of structure was chosen, since it has already been closely investigated. It is therefore well described in literature and analytical formulas for verification exist.

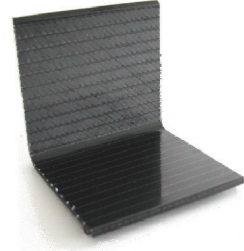


Figure 2: CFRP L-profile test specimen

1.1. Phenomenon Spring-In

Main reason for spring-in on a composite L-profile is the anisotropic material property. Chemical shrinkage as well as thermal expansion in fibre direction are much lower than in perpendicular direction. Assuming the radial effects much higher than tangential shrinkage will cause outer fibres to move to smaller radii and inner fibres to move to greater radii, as depicted in Figure 3. This leads to compression in the outer fibres and tension in the inner fibres. Assuming furthermore, that the fibres are sufficiently stiff, a certain spring in angle $\Delta\theta$ will be generated.

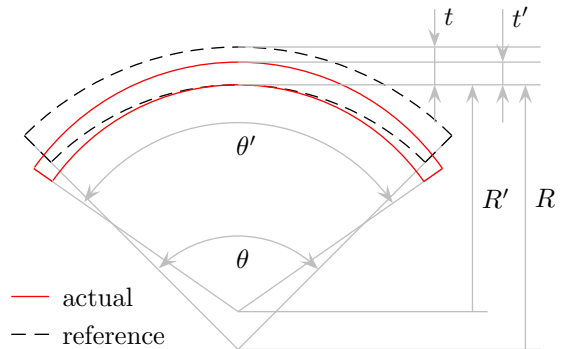


Figure 3: Spring-in

The spring-in angle can be expressed as the difference between the actual and the reference angle and it can be divided into a thermal and a chemical fraction as shown in Equation (1).

$$\Delta\theta = \theta' - \theta = \Delta\theta_{th} + \Delta\theta_{ch} \quad (1)$$

In accordance with [8] and [9] this circumstance leads to the analytical equation for spring-in angle for an orthotropic material.

$$\Delta\theta = \theta \cdot \left[\left(\frac{\alpha_t - \alpha_r}{1 + \alpha_r \cdot \Delta T} \right) + \left(\frac{\phi_t - \phi_r}{1 + \phi_r} \right) \right] \quad (2)$$

Herein $\Delta\theta$ being the spring-in angle, θ the original structure angle (90° in the present study), α_r , α_t the radial and tangential coefficient of thermal expansion (CTE), ϕ_r , ϕ_t the radial and tangential chemical shrinkage and ΔT the process temperature difference respectively.

In general it is possible to differentiate two kinds of spring-in shape changes. On the one hand there are global deformations of initially curved parts and on the other hand there are shape changes in the cross section of the part. Because of this circumstance the separation in global and local spring-in effects as depicted in Figure 4 are useful.

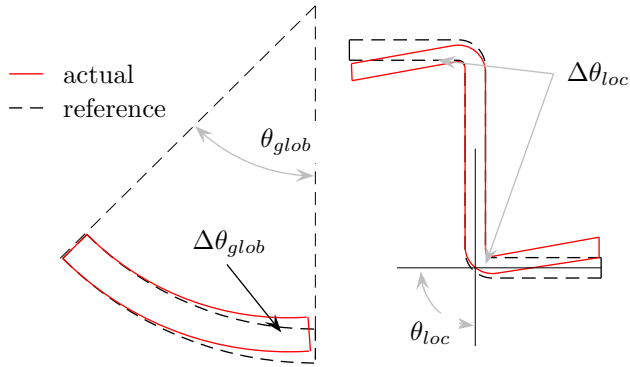


Figure 4: Separation of global and local spring-in deformations ($\Delta\theta_{glob}$ and $\Delta\theta_{loc}$) of a z-profile.

Regarding a typical aircraft spar, manufacturing induced variation of the global spar radius is a typical example of global spring-in. Shape deformations of the cross section are typically referable to local spring-in.

1.2. Phenomenon warpage

Different CTEs (*Coefficient of Thermal Expansion*) of tool and part as well as autoclav pressure are significant parameters which are responsible for the evolution of warpage on processes using singleside moulds. Due to pressure and high temperature during modern autoclav processing the transmission of shear stresses caused by tool expansion is supported. According to Fernlund [6] this leads to a through thickness stress gradient with tension at the mouldside of the part. After completion of processing these stresses relax which causes warpage of the flat part. Figure 5 shows a constitutive scheme of this phenomenon. Because of the use of Ni36 as toolmaterial, which has a similar CTE as the composite part, and because of the usage of a double sided mould in the RTM process it was possible to blank out effects of warpage as far as possible in the investigation of the spring-in. The present study therefore concentrates on the spring-in phenomenon with focus to the influence of different process-characteristics.

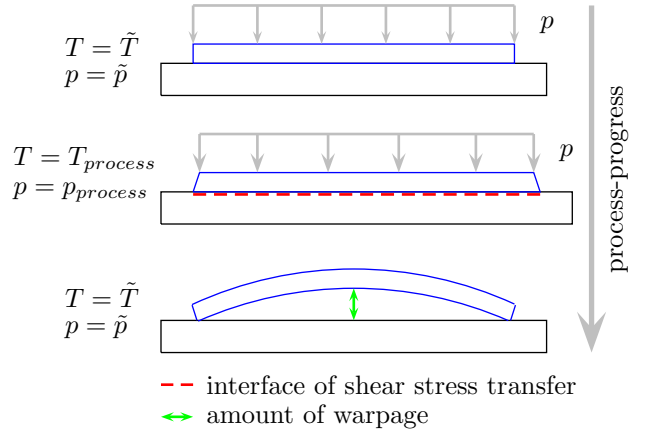


Figure 5: Warpage of flat composite parts due to internal stresses ($CTE_{tool} > CTE_{part}$)

2. Determination of relevant Materialparameters

2.1. Preliminary remarks

Dealing with fibre-composite materials requires to know the parameters of the single constituents. The laminate of the L-profile in this study consists of HTS-fibers from TOHO/TENAX and the RTM6 matrix system from HEXCEL. All data is taken from literature [10]-[16] The parameters of an uni-directional single ply are calculated using ESAComp 3.4. As reference a laminate with a fibre volume fraction (FVF) of 60% is considered. All data are listed in table 1.

Table 1 – Material properties of HTS/RTM6 unidirectional single ply

Properties	Value	Unit
E_{11}	143960	MPa
$E_{22} = E_{33}$	5955	MPa
$G_{12} = G_{13}$	2485	MPa
G_{23}	2235	MPa
$\nu_{12} = \nu_{13}$	0.26	–
ν_{23}	0.33	–
Density ρ	1512	kg/m ³

Since the CTE of the constituents turned out to be the most unreliable data, a numerical study investigating their influence on the spring-in behaviour was conducted. It could be shown, that the CTE of the matrix dominates the mechanical behaviour of the laminate. In the present study this parameter is used to equalize measurement and simulation results. In the following this parameter is named equivalent CTE and is defined as sum of thermal and chemical shrinkage related to the process temperature difference (derivation of Equation (3) can be found in the appendix).

$$\alpha_{mequ} = \alpha_{m_{therm}} + \alpha_{m_{chem}} = \alpha_{m_{therm}} + \frac{\Delta V_{chem}}{3 \cdot \Delta T} \quad (3)$$

Four different processes were investigated. All leading to a temperature difference of $\Delta T = 160K$ coming from $180^\circ C$ highest process temperature and $20^\circ C$ room temperature.

P1 (nominal) - gelation $130^\circ C$ / curing $180^\circ C$

P2 (max shrink) - gel. / cure $180^\circ C$

P3 (mid shrink) - long gel. $130^\circ C$ / cure $180^\circ C$

P4 (low shrink) - long gel. $110^\circ C$ / cure $180^\circ C$

P1 is a nominal industrial process. P2 is the process with the highest shrinkage, since a fast gelation at high temperature prevents a shrinkage compensation by liquid resin. Processes P3 and P4 have a lower shrinkage due to their long gelation time at lower temperatures.

This is caused by the slow change from liquid to solid state allowing the compensation of the shrinkage by liquid resin. As assumption the process P4 is considered as a process without chemical shrinkage which means, that the equivalent CTE will have a thermal term only. The value of the thermal term will be equal for the remaining three processes. Hence the difference will be the fraction coming from the chemical shrinkage.

2.2. L-profile FE-model

To predict the spring-in properly it is mandatory to account for the thickness effect as it is described in section 1.1. Hence the L-profile was modelled with solid (HEX8) elements using MSC/Patran (see Fig. 6). The test structures were made from a $2mm$ laminate with 8 NCF (*Non-Crimp Fabric*) single plies ($t = 0.125mm$) and a symmetrical lay-up of $[4 \times \pm(45^\circ)]$. The inner radius of the L-profile is $5mm$.

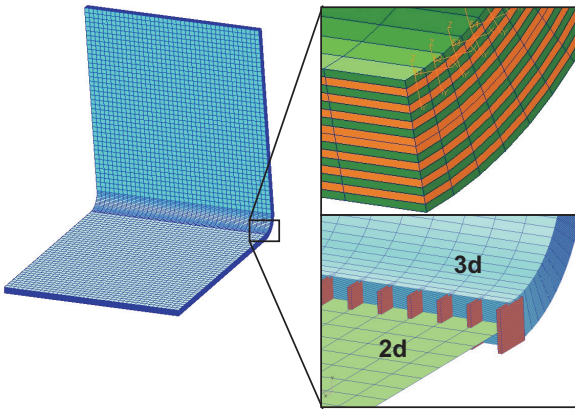


Figure 6: CFRP L-profile FE-modelling

In the FE model each single ply needs to be modelled with at least three elements over its thickness. With this requirement and in order to avoid elements with bad aspect ratios an extremely fine mesh is required leading to an enormous number of DoF (*Degrees of Freedom*) even for comparably small structures like the L-profile. Therefore the capability of a hybrid modelling was investigated.

In this case the thickness effect is accounted for by using HEX8 elements (3D-orthotropic material) only locally in the zone of the radius. The remainders of the structure are modelled with QUAD4 shell elements (2D-orthotropic material) as can be seen in Fig. 6. This leads to the reduction of the DoF enabling the analysis of large, thin-walled composite structures. The interface between solid and shell elements is modeled with stiff bar elements to prevent warping at the free edges of the solid area while shrinkage in transversal direction is not constrained. Combined 2D-3D analysis yields almost identical spring-in results as for 3D-3D. In this study each structure was analyzed under two different conditions. First, iso-static mounting to obtain free internal stresses and the corresponding deformations. Second, in-service mounting conditions to calculate stress in superimposed condition of internal and mounting loads.

2.3. L-profile FE Analysis and Results

In the analyses the matrix CTE was adjusted such, that the spring-in angles are equal to the experimentally gained ones for a FVF = 60%. All other FVF from 55% to 70% were conducted to check the reliability of the method. In Fig. 7 there are shown measured and analyzed spring-in angles related to the norm process P1 and a FVF = 60%. As previously defined the process P4 shall be a zero-chemical shrinkage process. Based on this the chemical volume shrinkage for the processes P2 - P4 varies between $0.68\% \leq \Delta V_{chem} \leq 3.25\%$. The corresponding shrinkage parameters namely the equivalent CTEs in fiber direction and perpendicular direction vary between $0.08 \cdot 10^{-6} K^{-1} \leq \alpha_{11} \leq 0.630 \cdot 10^{-6} K^{-1}$ and $36.80 \cdot 10^{-6} K^{-1} \leq \alpha_{22}, \alpha_{33} \leq 63.27 \cdot 10^{-6} K^{-1}$.

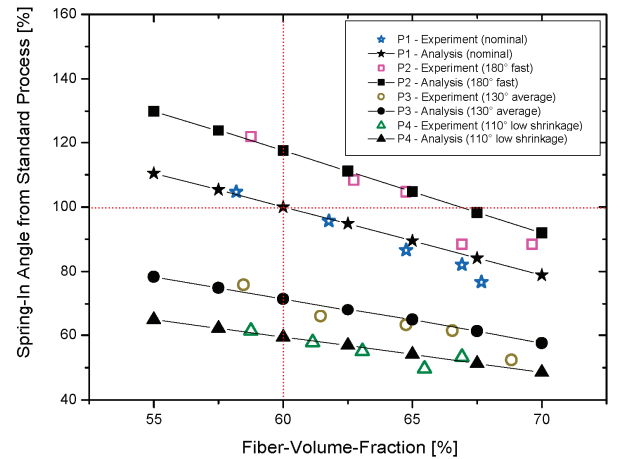


Figure 7: Comparison of measured and calculated spring-in results

The results coming from Equation (3) by using the gained shrinkage data of a uni-directional single ply leads to approx. 25% lower spring-in results as experimentally measured. Even by using the pure thermal CTE for P4 the results do not lead to comparable values. The experimentally measured values of the spring-in however correspond

to data gained by Darrow [4]. The spring-in results gained by using the hybrid FE modelling are in very good agreement with the fully 3D modelled L-profile. It therefore is considered to be suitable for the analysis of a large, thin-walled composite structure.

In terms of stresses the process P2 resembles the process with the highest chemical shrinkage and hence highest eigenstresses. Under iso-static mounting conditions the matrix has a tension load of $\approx 68MPa$ and it follows trivially that the fibers have a compression load of the same magnitude. In fixed configuration the stresses are ranging from $-158MPa$ in the fibers of the outer radius and $\approx 66MPa$ in the matrix of all layers. Here the gained results need some more discussion. Especially the magnitude of tensile strength in the matrix system needs to be investigated more thoroughly. As a remark it shall be mentioned, that the induced stresses in the nominal process P1 are about half of the before described P2.

3. Analysis of Curved Airframe Structure

3.1. Preliminary Remarks

For a spring-in analysis of a large, thin-walled structure it becomes obvious, that a full solid modelling is not manageable in terms of model sizes and hence computational effort. Therefore the approach of hybrid modeling is transferred from L-profile level to a larger airframe structure. All material properties determined within the L-profile investigations are used for this large scale application which is, stiffness and shrinkage properties as outlined in previous paragraphs. As a measure of the analysis results the computed spring-in of the global radius of a curved Z-profile as shown in Fig. 8 was compared to experimentally gained data.

3.2. FE-Model of Curved Airframe Structure

A Z-shaped generic frame structure as depicted in Fig. 8 with a global curvature radius of $\approx 2m$, a length of $\approx 2.5m$ and a variable profile height between $90mm$ and $120mm$ was subject of the investigations. The same material properties as for the L-profile were used and the profile is manufactured according to process P1, the norm process.

The web is composed of 8 uni-directional single plies with a thickness of $t = 0.25mm$ and a $[2 \times (\pm 45)]_S$ lay-up with a total thickness of $2.0mm$. 13 plies are foreseen alternatively in the inner and outer chord with a lay-up of $[(+45/-45/0)_S/0/(+45/-45/0)_S]$ and a total thickness of $3.25mm$.

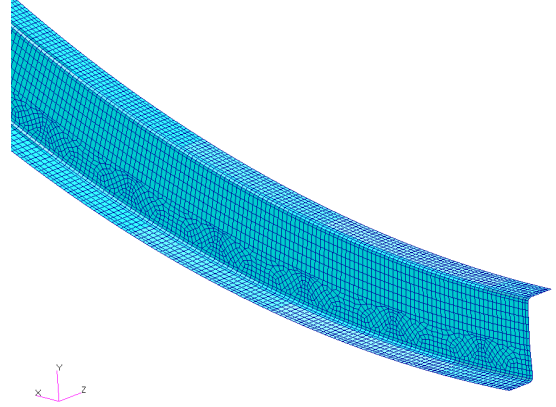


Figure 8: Curved frame Z-profile

In order to determine the free eigenstresses and the global spring-in the Z-profile was iso-statically fixed at one free end. Therewith avoiding that the web can change its global orientation and additional stresses are induced (see Fig. 9 left). The fixation in in-service position is such, that the outer chord can move along the circumferential line of the global radius but all other movements are prevented as can be seen on the right picture of Fig. 9.

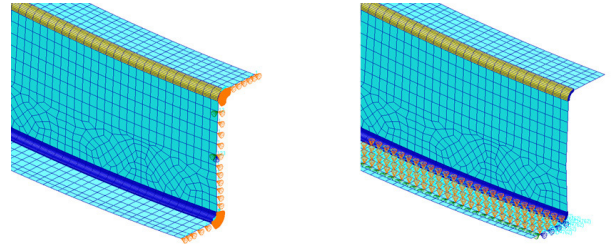


Figure 9: Mounting of Z-frame for spring-in analysis

As earlier mentioned the pure 3D modelling leads to a very high number of DoFs already for comparably small structures. Therefore three different model types were analysed and evaluated:

1. Model created from shell elements: Assuming that global spring-in is driven by shrinkage of the web, representing the transversal shrinkage and thereby forcing the belts to move to other radii which causes the spring-in effect.
2. Hybrid model with solid elements between web and inner chord: Assuming the same effect as in 1. and by consideration of the spring-in in the radius between web and inner chord.
3. Hybrid model with solid elements between web and both chords: Assuming the same effect as in 1. and by consideration of the spring-in in both radii between web and chords.

3.3. Z-profile Analysis and Results

In this section the analysis results in terms of spring-in of the global profile radius and stresses will be dealt

with. The principle behaviour of the investigated structure wrt. to its lay-up in the inner and outer chords is shortly discussed.

Figure 10 shows the Z-profile with a slightly decreased global radius together with some torsion of the profile. This mode will occur with unidirectional layers in either both chords or only in the outer chord. In case of unidirectional layers in the inner chord this kind of profile would "spring-out" due to different CTEs between inner and outer chord. The inner chord with its low CTE and high stiffness would remain almost unchanged whereas the outer chord with its high CTE would open the curved structure.

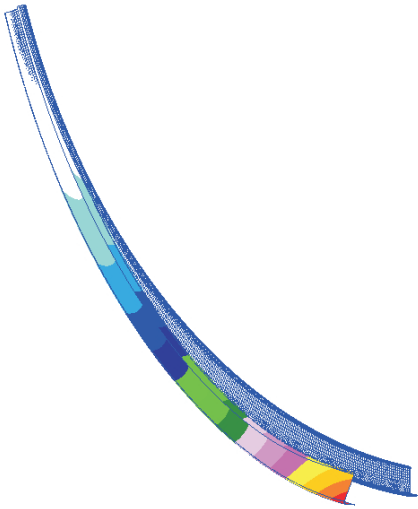


Figure 10: Deformed shape of Z-profile after manufacturing

The before mentioned three different model types of generic frame structure with different considerations of the relevant spring-in zones were investigated at first. It became obvious, against expectations, that the global spring-in is driven by the local spring-in in the radii between web and chords. This holds especially true, if there are longitudinal layers foreseen in the chords, which provide a high stiffness and low shrinkage in profile longitudinal direction. In the case there are no longitudinal layers foreseen in a chord it may be possible to save a 3D modelling in this zone but it depends very much on the design of the structure and the chosen material. However, all results that will be presented hereafter are gained from a model considering all local thickness effects.

In Table 2 there are listed the global spring-in radii, that were analyzed with the different process parameters, as well as the global spring-in radius of the manufactured part using process P1. It can be seen, that the data fit quite well with the measured ones. Furthermore, it becomes obvious that the difference between the processes P1 (nominal) and P2 (fast) is smaller than comparing P1

with P3 and P4. In case of the last-mentioned a more significant decrease of spring-in can be noticed compared to P1. Processes P3 and P4 seem to be advantageous from quality point of view but these processes require 1.5 to 2 times longer process times, which on the other hand is disadvantageous in the sense of the achievement of high manufacturing rates.

Table 2 – Spring-in of global radius of curved airframe structure

Process	Global Radius	Difference to norm process
produced (P1)	1963.5 mm	0.0 mm
P1	1964.5 mm	1.0 mm
P2	1963.0 mm	-0.5 mm
P3	1967.1 mm	3.6 mm
P4	1968.9 mm	5.4 mm

In the following Table 3 all stresses gained from the isotatic configuration are listed for processes P1 and P2 for comparison. Hereby the stresses are evaluated in fiber and matrix direction and distinguished between chords and frames. It can be found that the stresses in the matrix material correspond to the values that were determined during the L-profile investigations. In most parts of the Z-profile the same can also be noticed for the fiber compression loads. In the radii between web and chords the stresses are slightly increased and in $\pm 45^\circ$ fibers of the inner chord a distinctive raise in the stresses becomes obvious. This is due to the specific deformation caused by the profile shape and of course due to the anisotropic material. Comparing the magnitude of stresses between the two processes it is noticeable, that the stresses of P2 are about twice as high as for the norm process. In the specific case of P1 and P2 the process times were equal. This underlines the high dependency of internal stresses from the way of curing.

Table 3 – Induced residual stresses in fiber and matrix

Stresses [MPa]		P1		P2	
		Min	Max	Min	Max
Fiber	Chords	-63	33	-125	65
	Frame	-33	53	-65	102
Matrix		30	34	58	70

All stresses that were analysed with the structure mounted in its in-service position show only marginal changes in the order of $\pm 3N/mm^2$. The changes of the stresses are once again very much dependent on the design of the structure and also on its mounting conditions. This becomes obvious when comparing the calculated low values of the generic frame structure with the results of the L-profile which are decisively larger.

It should be mentioned that the calculated matrix stress-

es even for the norm process P1 are extremely close to typical failure loads of epoxy resins. This topic needs more detailed investigations to allow save design under consideration of manufacturing issues. One way of investigating the severity, could be the monitoring of micro cracks after demoulding.

4. Summary & Outlook

A way is presented which allows for the determination of spring-in deformations and eigenstresses of large, thin-walled CFRP structures based on linear-static FE simulations. Furthermore this approach allows for the prediction of stresses inside the structures in mounted position including prior determined eigenstresses. All analyses within this study are linear static and were performed using MSC/Nastran.

All mechanical properties of the single laminate constituents were extracted from literature and the properties of the unidirectional single plies were analysed using ESAComp3.4. Thermal and chemical shrinkage were determined by comparing test results on CFRP L-profiles with analysis results based 3D FE models representing each single layer of the structure. Test results gained from the process with low chemical shrinkage were used to determine the thermo-elastic contribution to the spring-in. For the remaining three tests the contribution of the chemical shrinkage was determined. The L-profile was reanalysed for a number of different fibre-volume fractions for validation reasons. The outcome in terms of displacements showed very good agreement with the test results. Concerning eigenstresses, comparably high values were found for the matrix material.

The pursued way of modelling leads to very large FE models. Therefore a simplification which combines 2D and 3D modelling was introduced. Those parts, where the transversal CTE leads to spring-in, are modelled conventionally using solid elements. All remaining parts, which are mainly flat, are modelled using shell elements. The application to the L-profile showed reasonable agreement and therefore this modelling technique was transferred to the simulation of a generic frame structure.

Studies with different modelling of the Z-profile showed that an adequate consideration of the radii between belts and web by 3D modelling are mandatory for reliable deformation predictions on large, thin-walled structures.

- **Interdisciplinary simulation**

In conjunction with the present work there are further aspects which have to be implemented into the simulation process. First there is the establishment of curing-simulation to determine the degree of cure and chemical shrinkage. An inhomogeneous field of temperature leads to an inhomogeneous field of cure and therefore highly nonlinear relations between deformations and stress-distribution.

Regarding the mentioned relations, investigations to enable such sophisticated simulation processes were conducted at the DLR. Reducing process time with regard to allowable stresses and deformations will be a big gain of an interdisciplinary simulation approach.

- **Tool-part interaction**

Another action item which is pursued at the DLR Institute of Composite Structures and Adaptive Systems is the enhancement of the presented simulation technique for singlesided mould manufacturing. For such processes warpage effects, which were blinded out in this study, must be considered as vital. Due to deformations of flanges as depicted in Figure 5 the simulation technique must be adjusted. With regard to curvature of flanges a full 3D analysis will be essential. Wang et al. [17] investigated the applicability of different element types with the result that a single layer of regular solid elements is suitable for the determination of spring-in deformations.

- **Aircraft-structures as usecase**

Beside the already mentioned shape-changes, which develop during the manufacturing process, another type of deformations caused by in-service loads require the enhancement of simulation techniques to enlarge its usage. Figure 11 points out a simple example for the result of poor dimensional control during the manufacturing process.

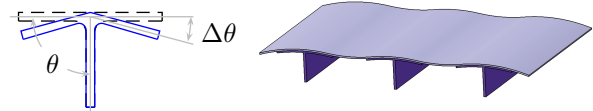


Figure 11: Wavy panel due to spring-in deformations of the stringers

To prevent surface waviness of stiffened panel structures it is essential to have good dimensional accuracy of stringers. Concerning high quality demands, as they are requested for laminar flows, for example, it is not sufficient to predict manufacturing deformations. In-service loads, like aerodynamical pressure on a wing surface, have a significant effect on the surface shape. Because of this fact investigations for combining CFD (*Computational Fluid Dynamics*) and FEM simulation are intended at the DLR.

Appendix

Volume-shrinkage as function of temperature

Nomenclature

V	actual-volume [m^3]
\tilde{V}	reference-volume [m^3]
$\tilde{a}, \tilde{b}, \tilde{c}$	reference-lengths [m]
a, b, c	actual-lengths [m]
ϵ_i	strain in i-direction [%]
λ_i	elongation in i-direction [%]
ϵ_V	volume-shrinkage [%]

$$\epsilon_V = \frac{\Delta V}{\tilde{V}} = \frac{V - \tilde{V}}{\tilde{V}} = \frac{V}{\tilde{V}} - 1 \quad (4)$$

$$\tilde{V} = \tilde{a} \cdot \tilde{b} \cdot \tilde{c} \quad \text{und} \quad V = a \cdot b \cdot c \quad (5)$$

$$a = \lambda_a \cdot \tilde{a} \quad \text{with} \quad \lambda_i = \epsilon_i + 1 \quad (6)$$

$$\epsilon_V = \frac{abc}{\tilde{a}\tilde{b}\tilde{c}} - 1 = \frac{\lambda_a \lambda_b \lambda_c \tilde{a}\tilde{b}\tilde{c} - \tilde{a}\tilde{b}\tilde{c}}{\tilde{a}\tilde{b}\tilde{c}} = \lambda_a \lambda_b \lambda_c - 1 \quad (7)$$

$$\epsilon_V = (\epsilon_a + 1)(\epsilon_b + 1)(\epsilon_c + 1) - 1 \quad (8)$$

$$\epsilon_V = \epsilon_a \epsilon_b \epsilon_c + \epsilon_a \epsilon_b + \epsilon_a \epsilon_c + \epsilon_b \epsilon_c + \epsilon_a + \epsilon_b + \epsilon_c \quad (9)$$

Assumption: isotropic material: $\epsilon_a = \epsilon_b = \epsilon_c = \epsilon$

$$\epsilon_V = \epsilon^3 + 3\epsilon^2 + 3\epsilon = 3\epsilon \cdot \left(1 + \epsilon + \frac{1}{3}\epsilon^2\right) \quad (10)$$

Equation 10 allows to express the volume shrinkage of isotropic material as a function of one-dimensional strain. Within typical amounts of volume shrinkage in the range of $1\% \leq \epsilon_V \leq 5\%$ it is possible to reduce equation 10 to $\epsilon \approx \frac{\epsilon_V}{3}$. For regarding chemical shrinkage as a function of temperature the following transformation is necessary.

$$\epsilon_{therm} = \alpha_{therm} \cdot \Delta T = \frac{\epsilon_V}{3} \rightarrow \alpha_{therm} = \frac{\epsilon_V}{3\Delta T} \quad (11)$$

References

- [1] Svanberg J. Magnus and Holmberg J. Anders. Prediction of shape distortions, Part 1. FE-implementation of a path dependent constitutive model. *Composite Part A: Applied Science and Manufacturing*, Vol. 35, Issue 6, June 2004, pp 711-721
- [2] Zhu Qui and Geubelle Philippe H. Dimensional accuracy of thermoset composites: shape optimization. *Journal of Composite Materials*, Vol. 36, No. 6, 2002, pp 647-672
- [3] Flores F., Gillespie Jr. J.W. and Bogetti T.A. Experimental investigation of the cure-dependent response of vinyl ester resin. *Polymer Engineering and Science*, Vol. 42, No. 3, March 2002, pp 582-590
- [4] Darrow A. David. Isolating components of processing induced warpage in laminated composites. *Journal of Composite Materials*, Vol. 36, 2002, pp 2407-2419
- [5] Sweeting R., Liu X.L. and Paton R. Prediction of processing-induced distortion of curved flanged composite laminates. *Journal of Composite Structures*, Vol. 57, 2002, pp 79-84
- [6] Albert C. and Fernlund G. Spring-in and warpage of angled composite laminates. *Composite Science and Technology*, Vol. 62, 2002, pp 1895-912

- [7] Svanberg J. Magnus. Prediction of shape distortion for a curved composite C-spar. *Journal of Reinforced Plastics and Composites*, Vol. 24, No. 3, 2005, pp 323-339
- [8] Radford D.W. and Rennick T.S. Separating sources of manufacturing distortion in laminated composites. *Journal of Plastics and Composites*, Vol. 19, No. 8, 2000, pp 621-641
- [9] Sproewitz T., Kleineberg M. and Tessmer J. Prozesssimulation in der Faserverbundherstellung – Spring-In. *NAFEMS Magazin Newsletter*, 1/2008, 9. edition
- [10] Hecxel Corporation. Product Sheet HexFlow RTM6 - 180°C epoxy system for resin transfer moulding monocomponent system
- [11] Hobbiebrunken T. Thermomechanical analysis of micromechanical formation of residual stresses and initial matrix failure in CFRP. *JSME International Journal*, Series A, Vol. 47, No. 3, 2004, pp 349-356
- [12] Holmberg J.A. Resin transfer moulded composite materials. Doctoral Thesis, *Luleå University of Technology*, Department of Materials and Manufacturing Engineering, Division of Polymer Engineering, Report 1997:10, 1997
- [13] TOHO TENAX Europe GmbH. Produktprogramm und Eigenschaften für TENAX® HTA/HTS Filamentgarn
- [14] Hull D. *An Introduction to Composite Materials*. University Press, Cambridge 1988
- [15] <http://www.torayca.com/techref/>
- [16] Callister W.D. *Material Science and Engineering an Introduction*. 3. edition, 1994
- [17] J.Wang, D.Kelly, W. *Finite Element Analysis of Temperature Induced Stresses an Deformations of Polymer Composite Components*, *Journal of Composite Materials*, Vol. 34 No. 17/2000, 1456-1471